

# Classes of hydrodynamic and magnetohydrodynamic turbulent decay

Axel Brandenburg<sup>1, 2, 3, 4, \*</sup> and Tina Kahnashvili<sup>5, 6, 7, †</sup>

<sup>1</sup>*Laboratory for Atmospheric and Space Physics, University of Colorado, Boulder, CO 80303, USA*

<sup>2</sup>*JILA and Department of Astrophysical and Planetary Sciences,  
University of Colorado, Boulder, CO 80303, USA*

<sup>3</sup>*Nordita, KTH Royal Institute of Technology and Stockholm University, Roslagstullsbacken 23, 10691 Stockholm, Sweden*

<sup>4</sup>*Department of Astronomy, AlbaNova University Center, Stockholm University, 10691 Stockholm, Sweden*

<sup>5</sup>*The McWilliams Center for Cosmology and Department of Physics,  
Carnegie Mellon University, 5000 Forbes Ave, Pittsburgh, PA 15213, USA*

<sup>6</sup>*Department of Physics, Laurentian University, Ramsey Lake Road, Sudbury, ON P3E 2C, Canada*

<sup>7</sup>*Abastumani Astrophysical Observatory, Ilia State University,  
3-5 Cholokashvili Ave, Tbilisi, GE-0194, Georgia*

(Dated: November 27, 2018, Revision: 1.40 )

We perform numerical simulations of decaying hydrodynamic and magnetohydrodynamic turbulence. We classify our time-dependent solutions by their evolutionary tracks in parametric plots between instantaneous scaling exponents. We find distinct classes of solutions evolving along specific trajectories toward points on a line of self-similar solutions. These trajectories are determined by the underlying physics governing individual cases, and not by the initial conditions, as is widely assumed. In the helical case, even for a scale-invariant initial spectrum (inversely proportional to wavenumber  $k$ ), the solution evolves along the same trajectory as for a Batchelor spectrum (proportional to  $k^4$ ). All of our self-similar solutions have an intrinsic subinertial range close to  $\propto k^4$ .

PACS numbers: 98.70.Vc, 98.80.-k

The study of *decaying* turbulence is as old as that of turbulence itself. Being independent of ill-defined forcing mechanisms, decaying turbulence might have a better chance in displaying generic properties of turbulence. Such properties are usually reflected in the existence of conserved quantities such as the Loitsianskii integral [1] and the magnetic helicity [2, 3]. Important applications of decaying turbulence include grid turbulence [4], turbulent wakes [5], atmospheric turbulence [6], as well as interstellar turbulence [7], galaxy clusters [8], and the early Universe [9, 10]. In the latter case, cosmological magnetic fields generated in the early Universe provide the initial source of turbulence, which leads to a growth of the correlation length by an inverse cascade mechanism [11], in addition to the general cosmological expansion of the Universe. In the last two decades, this topic has gained significant attention. The time span since the initial magnetic field generation is enormous, but it is still uncertain whether it is long enough to produce fields at sufficiently large length scales to explain the possibility of contemporary magnetic fields in the space between clusters of galaxies [12].

In this Letter, we use direct numerical simulations (DNS) of both hydrodynamic and magnetohydrodynamic (MHD) decaying turbulence to classify different types by their decay behavior. The decay is characterized by the temporal change of the kinetic and magnetic energy spec-

tra,  $E_K(k, t)$  and  $E_M(k, t)$ , respectively. Here,  $k$  is the wavenumber and  $t$  is time. In addition to the decay laws of the energies  $\mathcal{E}_i(t) = \int E_i(k, t) dk$ , with  $i = K$  or  $M$  for kinetic and magnetic energies, there are the kinetic and magnetic integral scales,

$$\xi_i(t) = \int_0^\infty k^{-1} E_i(k, t) dk / \int_0^\infty E_i(k, t) dk. \quad (1)$$

We quantify the decay by the instantaneous scaling exponents  $p(t) \equiv d \ln \mathcal{E} / d \ln t$  and  $q(t) \equiv d \ln \xi / d \ln t$ . Thus, we study the decay behaviors by plotting  $p(t)$  vs.  $q(t)$  in a parametric representation. The  $pq$  diagram turns out to be a powerful diagnostic tool.

Earlier work [8, 13, 14] has suggested that the decay behavior, and thus the positions of solutions in the  $pq$  diagram, depend on the exponent  $\alpha$  for initial conditions of the form  $E \sim k^\alpha e^{-k/k_0}$ , where  $k_0$  is a cutoff wavenumber. Motivated by earlier findings [2, 11] of an inverse cascade in decaying MHD turbulence, Olesen considered the time-dependent energy spectra  $E(k, t)$  to be of the form [14]

$$E(k, t) \propto k^\alpha \psi(k \xi(t)), \quad (2)$$

where  $\xi(t) \propto t^{1/q}$ , with  $q$  being an as yet undetermined scaling exponent, and  $\psi$  is a function that depends on the dissipative and turbulent processes which must lead to a departure from a pure powerlaw at large  $k$ . Moreover,  $\psi$  must obey the boundary condition  $\psi(0) = 1$ . This turns out to be a critical restriction.

Olesen then makes use of the fact that the hydrodynamic and MHD equations are invariant under rescal-

\*Electronic address: brandenb@nordita.org

†Electronic address: tinatin@andrew.cmu.edu

ing,  $x \rightarrow \tilde{x}\ell$  and  $t \rightarrow \tilde{t}\ell^{1/q}$ , which implies corresponding rescalings for velocity  $u \rightarrow \tilde{t}\ell^{1-1/q}$  and viscosity  $\nu \rightarrow \tilde{\nu}\ell^{2-1/q}$ . Furthermore, using the fact that the dimensions of  $E(k, t)$  are given by  $[E] = [x]^3[t]^{-2}$ , and requiring  $\psi$  to be invariant under rescaling  $E \rightarrow \tilde{E}\ell^{3-2/q} \propto \tilde{k}^\alpha \ell^{-\alpha} \psi$ , he finds from Eq. (2) that  $\alpha = -3 + 2/q$ . One therefore expects that for a given subinertial range spectral exponent  $\alpha$ , the exponent  $q$  is given by [14–17]

$$q = 2/(3 + \alpha). \quad (3)$$

This relation is independent of physical conditions such as the initial magnetic and kinetic energy spectra and the presence or absence of kinetic or magnetic helicity. A remarkable prediction of Olesen's work concerns the existence of inverse transfer even in the absence of magnetic helicity, provided  $\alpha > -3$ .

In this Letter, we argue that the scaling exponent  $q$  is *not* determined by the initial value of  $\alpha$ , as suggested by Eq. (3), but by the physical processes involved. Moreover, we relax the restriction  $\psi(0) = 1$  and write instead

$$E(k\xi(t), t) = \xi^{-\beta} \phi(k\xi), \quad (4)$$

where  $\xi = \xi(t)$  is computed from Eq. (1) and  $\beta$  needs to be determined empirically or theoretically. Clearly, the initial powerlaw slope at small  $k$  is no longer an adjustable input parameter, but is fixed by the form of  $\phi = \phi(\kappa)$ , where  $\kappa = k\xi$ . Specifically, the “intrinsic” slope is  $\alpha_0 \equiv d \ln \phi / d \ln \kappa$ . Evidently,  $\psi$  can be computed from  $\phi$  as  $\psi(\kappa) = \xi^{\alpha-\beta} \phi(\kappa) / \kappa^\alpha$ , but in general this  $\psi$  no longer satisfies  $\psi(0) = 1$ .

In the following, we explore examples of different decay behaviors in the diagnostic  $pq$  diagram using data from DNS. As in earlier work [18], we solve the nonideal MHD equations for an isothermal equation of state, i.e., pressure  $P$  and density  $\rho$  are proportional to each other,  $P = \rho c_s^2$ , where  $c_s = \text{const}$  is the sound speed. The magnetic diffusivity  $\eta$  is chosen to be equal to the kinematic viscosity  $\nu$ , whose value is characterized by the Reynolds number,  $\text{Re} = u_{\text{rms}} \xi / \nu$ . The governing equations are solved using the PENCIL CODE [19]. The resolution is typically  $2304^3$  meshpoints. The Mach number  $u_{\text{rms}}/c_s$  is always below unity, so compressibility effects are weak.

We first consider cases that all have  $\alpha = 4$  for the initial spectral slopes of  $E_K$  or  $E_M$ . We consider (i) hydrodynamic decay, (ii) nonhelical MHD decay, and (iii) helical MHD decay. In cases (ii) and (iii), the magnetic energy also drives kinetic energy through the Lorentz force. The particular simulation of case (ii) was already presented in Ref. [20], where inverse transfer to smaller wavenumbers was found in the absence of magnetic helicity using high-resolution DNS. Case (iii) leads to standard inverse transfer [2, 3, 9, 10]. The resulting spectra are plotted in Figs. 1(a)–(c), where we show energy spectra for cases (i)–(iii) at different times. The values of  $\text{Re}$  at half time are roughly 100, 230, and 300, respectively.

TABLE I: Scaling exponents and relation to physical invariants and their dimensions.

$\beta$	$p$	$q$	inv.	dim.
4	$10/7 \approx 1.43$	$2/7 \approx 0.286$	$\mathcal{L}$	$[x]^7[t]^{-2}$
3	$8/6 \approx 1.33$	$2/6 \approx 0.333$		
2	$6/5 = 1.20$	$2/5 = 0.400$		
1	$4/4 = 1.00$	$2/4 = 0.500$	$\langle \mathbf{A}_{2D}^2 \rangle$	$[x]^4[t]^{-2}$
0	$2/3 \approx 0.67$	$2/3 \approx 0.667$	$\langle \mathbf{A} \cdot \mathbf{B} \rangle$	$[x]^3[t]^{-2}$

In Figs. 1(d)–(f) we compare with suitably compensated spectra. We compensate for the shift in  $k$  by plotting  $E(k, t)$  against  $k\xi(t)$ . This implies that the peak in each spectrum, which is approximately at  $k = \xi^{-1}$ , will always have the same position on the abscissa. Furthermore, to compensate for the decay in energy, we multiply  $E$  by  $\xi^\beta$  with some exponent  $\beta$  such that the compensated spectra collapse onto a single function  $\phi(k\xi(t)) \approx \xi^\beta E(k\xi(t), t)$ .

Let us now consider solutions (i)–(iii) in the  $pq$  diagram; see Figs. 2(a)–(c). To study the relation between the exponents  $\beta$  and  $q$ , we make use of Olesen's scaling arguments and that  $\phi$  should be invariant under rescaling, to show from Eq. (4) that  $\beta + 3 - 2/q = 0$ , i.e.,

$$\beta = 2/q - 3, \quad (5)$$

or  $q = 2/(3 + \beta)$ . This is formally equivalent to Olesen's relation (3), but with  $\alpha$  being replaced by  $\beta$ . Moreover, unlike the exponent  $\alpha$  in Eq. (2), the exponent  $\beta$  in Eq. (4) bears no relation with the initial spectral slope. Correspondingly, the temporal decay of kinetic and magnetic energies follows power laws  $\mathcal{E}_i(t) \sim t^{-p_i}$  for  $i = \text{K or M}$ . The exponents are obtained by integrating the spectra over  $k$ ,  $\mathcal{E}(t) \equiv \int E(k, t) dk = \xi^{-(\beta+1)} \int \phi d(k\xi) \propto t^{-p}$ , and since  $\xi \propto t^q$ , this yields

$$p = (1 + \beta) q. \quad (6)$$

Thus, in a  $pq$  diagram, a certain value of  $\beta$  corresponds to a line  $p(t) \propto q(t)$  with the slope  $\beta + 1$ . Furthermore, inserting Eq. (5) yields the line  $p = 2(1 - q)$ . In a  $\beta q$  diagram, this line is directly given by Eq. (5); see Figs. 2(d)–(f). We call this the self-similarity line. Here,  $\beta(t)$  has been obtained directly from  $d \ln \mathcal{E} / d \ln \xi \equiv \beta(t) + 1$ .

The exponents  $\beta$ ,  $p$ , and  $q$  are roughly consistent with those expected based on the dimensions of potentially conserved quantities such as the Loitsianskii integral [21],  $\mathcal{L} = \int \mathbf{r}^2 \langle \mathbf{u}(\mathbf{x}) \cdot \mathbf{u}(\mathbf{x} + \mathbf{r}) \rangle d\mathbf{r} \propto \ell^5 u_\ell^2$ , with typical velocity  $u_\ell$  on scale  $\ell$ , the magnetic helicity,  $\langle \mathbf{A} \cdot \mathbf{B} \rangle$ , where  $\mathbf{B} = \nabla \times \mathbf{A}$  is the magnetic field in terms of the vector potential  $\mathbf{A}$ , and the mean squared vector potential,  $\langle \mathbf{A}^2 \rangle$ , which is conserved in two-dimensions (2D); see Table I.

In the hydrodynamic case (i), the solution approaches the  $\beta = 3$  line and then settles on the self-similarity line

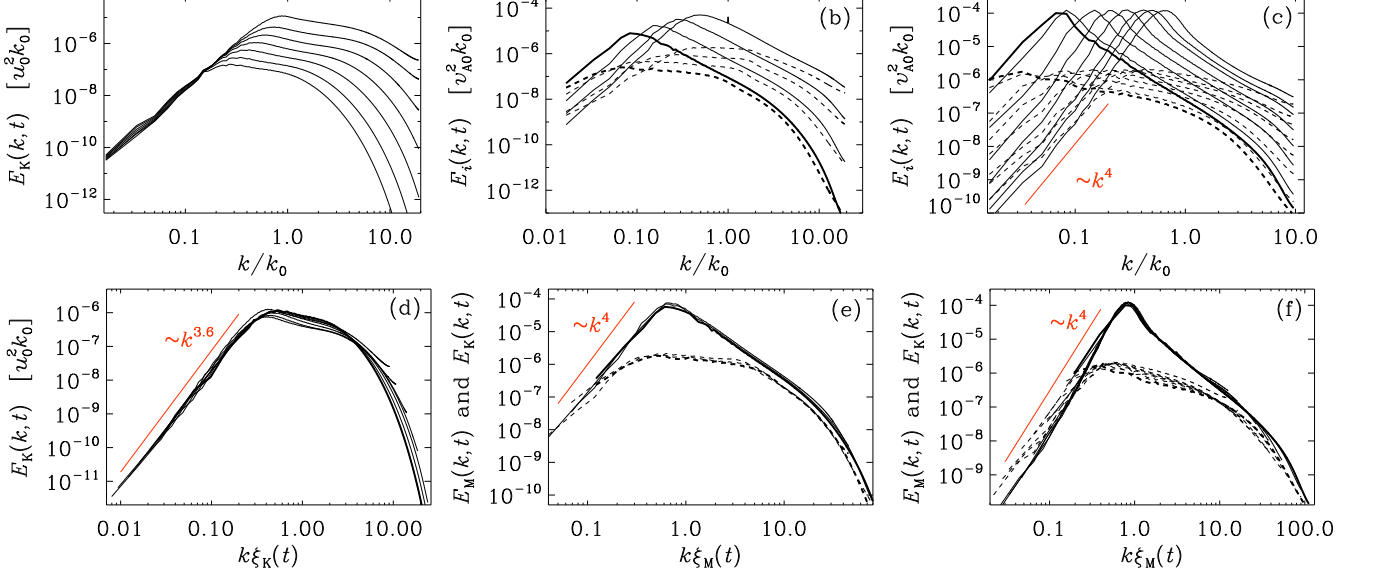


FIG. 1:  $E_K(k, t)$  for different  $t$  in a hydrodynamic DNS (a), compared with  $E_M$  (solid) and  $E_K$  (dashed) in MHD without helicity (b), and with (c). Panels (d)–(f) show collapsed spectra using  $\beta = 3$  (d),  $\beta = 1$  (e), and  $\beta = 0$  (f).

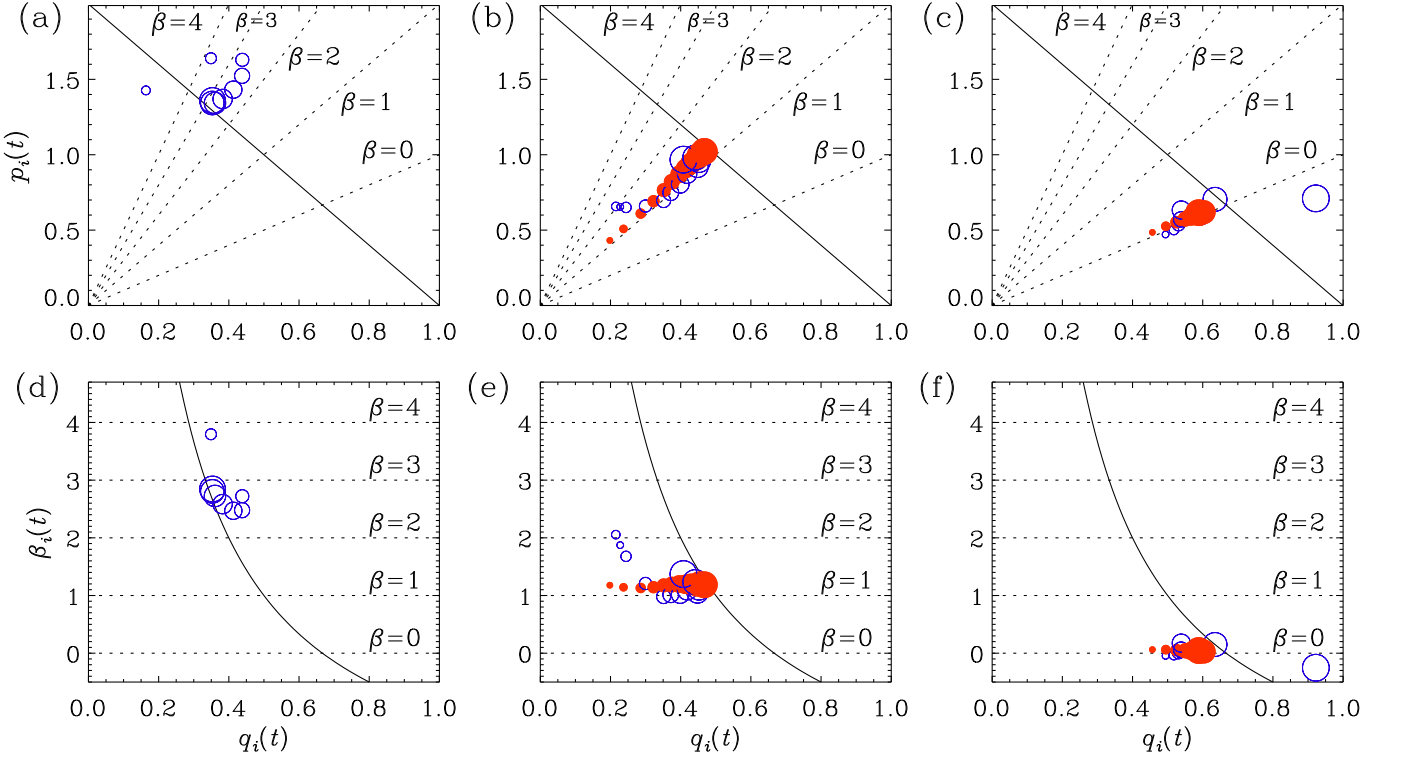


FIG. 2:  $pq$  diagrams for the cases (i)–(iii) shown in Fig. 1. Panels (d)–(f) show the corresponding  $\beta q$  diagrams. Open (closed) symbols corresponds to  $i = K$  (M) and their sizes increase with time.

at  $q \approx 1/3$ ; see Figs. 2(a) and (d). This decay behavior departs from what would be expected if the Loitsianskii integral were conserved, i.e.,  $q = 2/7$  and  $\beta = 4$ . The difference between  $\beta = 3$  and 4 is maybe not significant and could be explained by small Reynolds number effects,

but it is possible that  $\mathcal{L}$  is not conserved in practice [1]. A slower decay law with  $p = 6/5$ , corresponding to  $q = 2/5$  and  $\beta = 2$  has been favored by Saffman [22], while experiments and simulations suggest  $p = 5/4$  [23, 24].

In case (ii), the solution evolves along  $\beta = 1$  toward

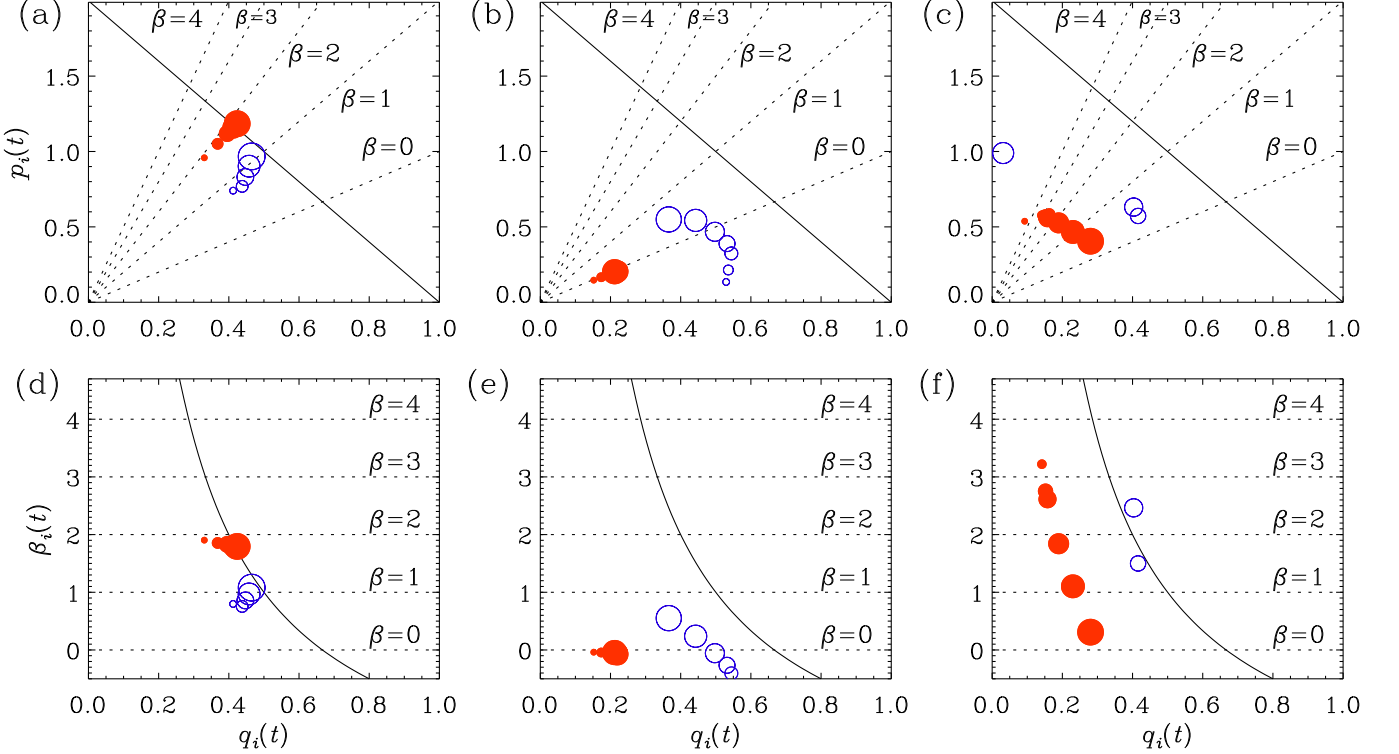


FIG. 3: Similar to Fig. 2, but for helical MHD turbulence with (a)  $\alpha = 2$  and (b)  $\alpha = -1$ , compared with (c) fractional helicity (6%) and again  $\alpha = -1$ . Panels (d)–(f) show the corresponding  $\beta q$  diagrams.

$q = 1/2$ ; see Figs. 2(b) and (e). This is compatible with the conservation of  $\langle \mathbf{A}_{2D}^2 \rangle$ , where  $\mathbf{A}_{2D}$  is the component of  $\mathbf{A}$  which describes the 2D magnetic field in the plane perpendicular to the local intermediate eigenvector of the rate-of-strain matrix; see the supplemental notes of [20] for details, and also [25]. The motivation for applying 2D arguments to 3D comes from the fact that for sufficiently strong magnetic fields the dynamics tends to become locally 2D in the plane perpendicular to the local field. This allows one to compute  $\mathbf{A}$  in a gauge that projects out contributions perpendicular to the intermediate eigenvector of the rate-of-strain matrix.

Finally, in case (iii) the solution evolves along  $\beta = 0$  toward  $q = 2/3$ ; see Figs. 2(c) and (f). This means that the spectrum shifts just in  $k$ , while the amplitude of  $E_M$  does not change, as can be seen from Fig. 1(c). This is consistent with the invariance of  $\langle \mathbf{A} \cdot \mathbf{B} \rangle$ ; see Ref. [3].

Next, we investigate cases with  $\alpha < 4$ . In particular, in the helical case with  $\alpha = 2$  we see that the subinertial range spectrum quickly steepens and approaches  $\alpha_0 = 4$ ; see Fig. 4(a). For  $\alpha = -1$ , which is a scale-invariant spectrum, the spectral energy remains nearly unchanged at small  $k$ , but the magnetic energy still decays due to decay at all higher  $k$ ; see Figs. 3(b) and (e). The values of  $p_M$  and  $q_M$  are rather small ( $\approx 0.2$ ), but the spectra can still be collapsed onto each other with  $\beta = 0$ ; see Fig. 4(e). However, in the nonhelical or weakly helical

case with  $\alpha = -1$ , the solution does not develop along  $\beta = \text{const}$  lines, but its trajectory is nearly parallel to the self-similarity line; see Figs. 3(c) and (f). The spectra no longer collapse onto each other; see Fig. 4(f). Furthermore, the exponents for  $i = K$  and  $M$  are quite different from each other.

All the examples discussed above demonstrate that  $\beta \neq \alpha$ , i.e., the self-similarity parameter is not determined by the initial power spectrum but rather by the different physical processes involved. The intrinsic slope  $\alpha_0$  associated with  $\phi$  is always found to be  $\approx 4$ ; this is independent of the value of  $\beta$ , which is 0 and 1 in helical and nonhelical MHD, and  $\approx 3$  in the hydrodynamic case.

In conclusion, the present work has revealed robust properties of the scaling exponent  $\beta$  governing the time-dependence of the energy spectrum  $E(k, t)$  through  $\xi^\beta \phi(k\xi)$  with a time-independent scaling function  $\phi$  and a time-dependent integral scale  $\xi(t)$ . Quite independently of the initial power spectrum  $\propto k^\alpha$  with different  $\alpha$  between 4 and  $-1$ , we always find that the magnetic and kinetic energy spectra collapse onto each other when  $\beta = 0$  in the helical case and  $\beta = 1$  in the nonhelical case. The helical case is particularly robust in that any point in the  $pq$  plane evolves along the  $\beta = 0$  line ( $p = q$ ) toward the point  $p = q = 2/3$ . Furthermore, if the initial spectrum has  $\alpha = 2$ , it first steepens to  $\alpha = 4$  and then follows the same decay as with an initial  $\alpha = 4$ . Moreover, for

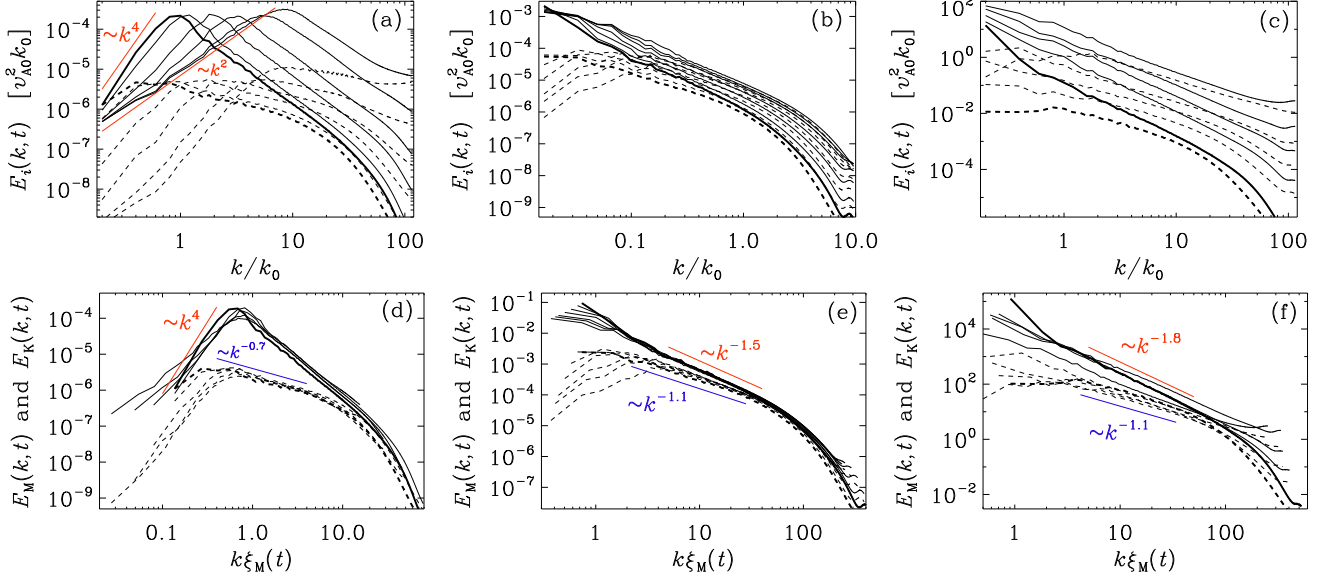


FIG. 4: Kinetic energy spectra in a hydrodynamic simulation (a), compared with magnetic (solid) and kinetic (dashed) energy spectra in a hydromagnetic simulation without helicity (b), and with (c). Panels (d)–(f) show the corresponding attempts to produce collapsed spectra using  $\beta = 0.4$  (d),  $\beta = 1$  (e), and  $\beta = 6$  (f).

a scale-invariant spectrum with  $\alpha = -1$ , we find again  $\beta = 0$ , i.e., the same as for  $\alpha = 2$  and 4, but now with  $p_M \approx q_M \approx 0.2$ ; see Fig. 3(b). In the fractionally helical case, points in the  $pq$  plane evolve toward the  $\beta = 0$  line and, for  $\alpha \geq 2$ , later toward  $p_M = q_M = 2/3$ .

We thank Andrey Beresnyak, Leonardo Campanelli, Ruth Durrer, Alexander Tevzadze, and Tanmay Vachaspati for useful discussions. Support through the NSF Astrophysics and Astronomy Grant Program (grants 1615940 & 1615100), the Research Council of Norway (FRINATEK grant 231444), the Swiss NSF SCOPES (grant IZ7370-152581), and the Georgian Shota Rustaveli NSF (grant FR/264/6-350/14) are gratefully acknowledged.

- [1] G. K. Batchelor and I. Proudman, *Phil. Trans. Roy. Soc. Lond. A*, **248**, 369 (1956).
- [2] A. Pouquet, U. Frisch, and J. Léorat, *J. Fluid Mech.* **77**, 321 (1976).
- [3] D. Biskamp and W.-C. Müller, *Phys. Rev. Lett.* **83**, 2195 (1999).
- [4] S. R. Stalp, L. Skrbek, and R. J. Donnelly, *Phys. Rev. Lett.* **82**, 4831 (1999).
- [5] I. P. Castro, *J. Fluid Mech.* **93**, 631 (1979).
- [6] D. K. Lilly, *J. Atmos. Sci.* **40**, 749 (1983).
- [7] M.-M. Mac Low, R. S. Klessen, and A. Burkert, *Phys. Rev. Lett.* **80**, 2754 (1998).
- [8] K. Subramanian, A. Shukurov, and N. E. L. Haugen, *Mon. Not. R. Astron. Soc.* **366**, 1437 (2006).
- [9] M. Christensson, M. Hindmarsh, and A. Brandenburg, *Phys. Rev. E* **64**, 056405 (2001).
- [10] R. Banerjee, K. Jedamzik, *Phys. Rev. D* **70**, 123003 (2004).
- [11] A. Brandenburg, K. Enqvist, and P. Olesen, *Phys. Rev. D* **54**, 1291 (1996).
- [12] Wagstaff, J. M. and R. Banerjee, *J. Cosmol. Astropart. Phys.* **01** (2016) 002.
- [13] W. K. George, *Phys. Fluids* **4**, 1492 (1992).
- [14] P. Olesen, *Phys. Lett. B* **398**, 321 (1997).
- [15] C. Kalelkar and R. Pandit, *Phys. Rev. E* **69**, 046304 (2004).
- [16] Campanelli, L., *Phys. Rev. D* **70**, 083009 (2004).
- [17] Campanelli, L., arXiv:1511.06797 (2015).
- [18] A. G. Tevzadze, L. Kisslinger, A. Brandenburg, T. Kahnishvili, *Astrophys. J.* **759**, 54 (2012).
- [19] <http://pencil-code.googlecode.com/>
- [20] A. Brandenburg, T. Kahnishvili, and A. G. Tevzadze, *Phys. Rev. Lett.* **114**, 075001 (2015).
- [21] P. A. Davidson, *J. Fluid Mech.* **663**, 268 (2010).
- [22] P. G. Saffman, *Phys. Fluids* **10**, 1349 (1967).
- [23] H. S. Kang, S. Chester, and C. Meneveau, *J. Fluid Mech.* **480**, 129 (2003).
- [24] N. E. L. Haugen and A. Brandenburg, *Phys. Rev. E* **70**, 026405 (2004).
- [25] P. Olesen, arXiv:1511.05007 (2015).